

Estimating Cenozoic Thickness in the Beijing Plain Area Using Array Microtremor Data

by Peifen Xu, Suqun Ling, Weiyan Ran, Qingxiao Liu, and Jinguang Liu

Online Material: Table of observation radius for microtremor measurements and inverted V_S structure.

INTRODUCTION

With the rapid expansion of large cities around the world, urban geological surveys provide key information regarding resource development and urban construction. Detailed geological information (e.g., sediment thickness, water table, bedrock structure, rock strength, faults, etc.) is critical to safeguarding large-structure stability and its operational safety. China's capital city, Beijing, is one of the largest cities around the world that possesses complex geological structures. Beijing ($N39.5^\circ \sim 41^\circ$, $E115.5^\circ \sim 117.5^\circ$) is located in the northern area of the Bohai Bay basin, which is surrounded by the Taihang Mountains fold belt to the west, Yanshan fold belt to the north, and Jiliao (Hebei–Liaoning) Rift basin to the southeast (Fig. 1). The structural pattern in the area was formed primarily by the Yanshan tectonic movement, which occurred during the mid-Jurassic to late Cretaceous. Because of the lack of major tectonic events during the Cenozoic period, the geological structure pattern in the area has remained almost unchanged, as evidenced by the topography seen today (mountainous area in the west and plain area in the east). Numerous major faults exist beneath the Beijing Plain area, acting as the major control factor of the well-known Beijing Rift Basin (Cai *et al.*, 2009). The west of the basin is enclosed by the Huangzhuang–Gaoliying fault followed by the Jingxi Uplift, and its east is adjacent to the Nanyuan–Tongxian fault followed by the Daxing Uplift. The resulting structural framework is characterized by two uplifts sandwiching a depression in the center (Jiao and Qiu, 2006; Cai *et al.*, 2009). The Beijing depression is further divided by smaller northwest–southeast faults, forming smaller structural highs and sags. From the southwest to northeast, there exist the Liangxiang High, Fengtai Sag, Laiguangying High, and Houshayu Sag (see Fig. 1; Luo *et al.*, 2008; Zhang and Lv, 2008).

The rock strata in the area are mainly composed of continental sediment dating from the Quaternary to Jurassic. The spatial distribution of the lithofacies and the shape of the geobodies are primarily controlled by the tectonic events discussed above. Earlier geological work has suggested considerable variations in the burial depth of pre-Tertiary bedrocks

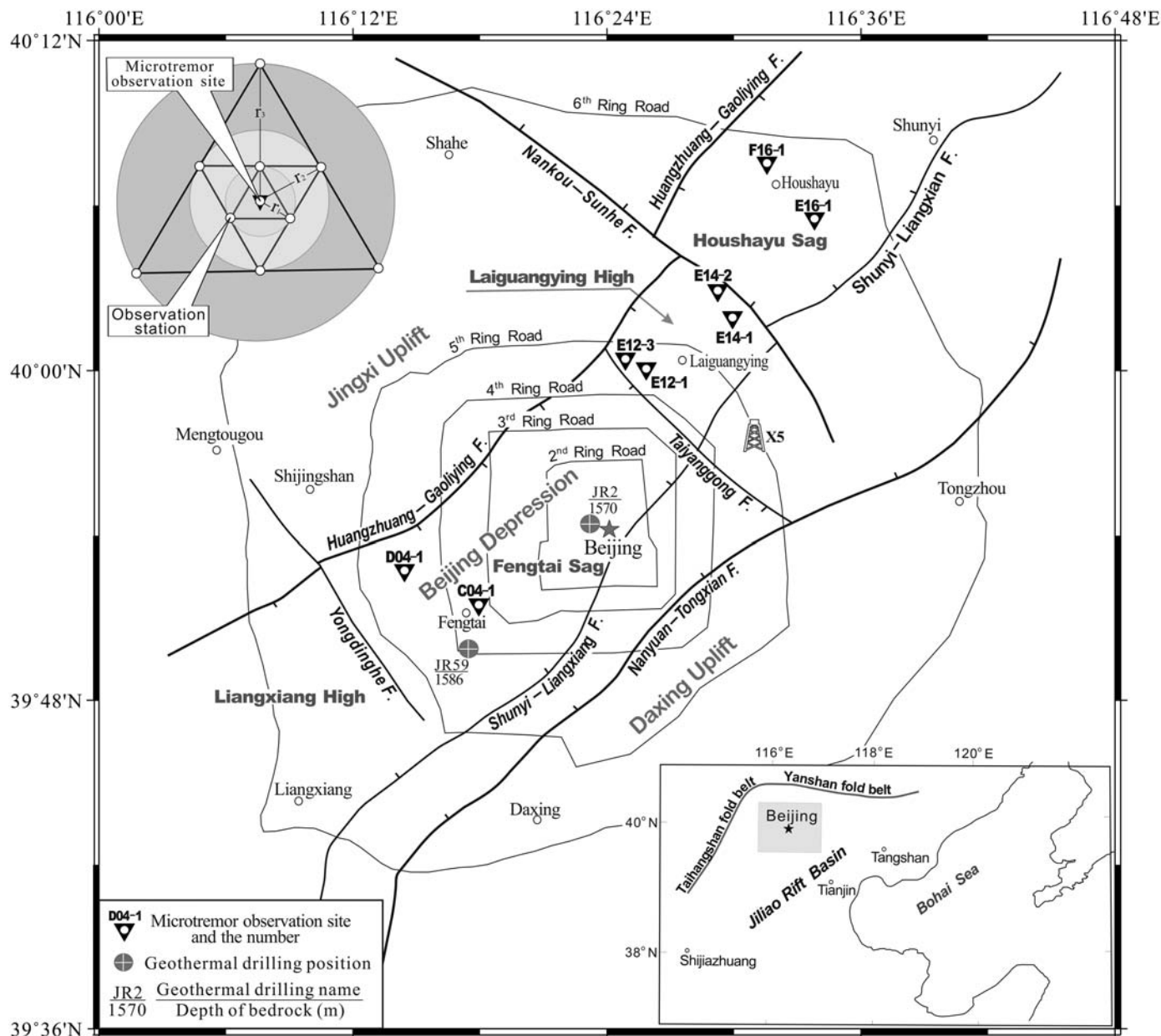
(Zhang and Lv, 2008; Cai *et al.*, 2009). Geological data from some geothermal wells drilled in the area were used to establish a 3D structure model for the bedrock. However, the lack of geological or geophysical data in some smaller areas significantly increased the uncertainty of the structure maps.

In this work, we collect and analyze microtremor data from eight observation sites using a microtremor-array survey method. The eight microtremor observation sites were located throughout the Fengtai Sag, Laiguangying High, and Houshayu Sag (Fig. 1). Traditional geophysical or geological survey methods were not effective in these areas due to the heavy traffic and dense buildings in the highly populated urban area. Here, we utilized the microtremor-exploration method (Okada *et al.*, 1987, 2003; Ling, 1994) at the eight observation sites to estimate the thickness of the Cenozoic sediments (or the bedrock depth) based on the shear-wave velocity profiles obtained through the surface-wave dispersion analysis.

MICROTREMOR METHOD

The microtremor exploration method is a Rayleigh-wave inversion technique that extracts its phase-velocity dispersion curve from the vertical component of the microtremor-array records, then inverts the shear-wave velocity structure (Aki, 1957, 1965; Ling, 1994; Ohori, 2002; Okada, 2003, 2006). Traditionally, two methods have been applied to estimate phase velocities from array records of microtremors. One is the frequency–wavenumber ($f-k$) spectral method (e.g., Horike, 1985; Matsushima and Okada, 1990; Kawase *et al.*, 1998), and the other is the spatial autocorrelation (SPAC) method (e.g., Aki, 1957; Okada *et al.*, 1987; Malagnini *et al.*, 1993). The SPAC method requires a circular configuration of the recording stations. The $f-k$ spectral method requires at least seven stations per array to produce stable inversion results (Okada *et al.*, 1990), which is quite difficult in downtown areas. However, the $f-k$ method has fewer restrictions in terms of array configurations compared with the SPAC method.

The bedrock surface in the Beijing area is characterized as a shear-wave velocity-contrast and lithologic boundary, which is located between the Cenozoic (Quaternary Q or Tertiary R) sediments/rocks and underlying Cretaceous or Jurassic bedrocks. This velocity contrast serves as the basis for estimating the bedrock depth using the microtremor-exploration method



▲ **Figure 1.** Map showing the major geological features of Beijing region (modified from Zhang and Lv, 2008; Ke, 2009b) and the SPAC microtremor observation sites. The black thick curved lines, major faults; the five-pointed star, center of Beijing; upper left illustration, the triple-circle observation-array system for the SPAC method used in this study; inset map, location of the study area.

and ensures the effectiveness of the method in this region. In fact, it has been recognized as one of the most attractive and convenient exploration methods for determining the S -wave velocity of sedimentary layers, especially in highly populated urban areas (e.g., Satoh *et al.*, 2001).

MICROTREMOR DATA ACQUISITION

The eight microtremor observation sites were situated in three different types of geological units (Fig. 1). Their latitude and longitude coordinates are provided in Table S1 (available as

an electronic supplement to this paper). In this study, we applied the SPAC method to estimate phase velocities from the array records of microtremors. The observation sensors were stationed in a circle with one common station at the center. The radius of a circular observation array (r) is known as the observation radius, which determines the targeted detection depth H . In general, the detection depth H is approximately 3–5 times the value of the observation radius r (Okada, 2003). The actual receiver array may consist of multiple microtremor observation circles with different radii. Here we used a triple circular receiver array system (shown in the upper left illustration of

Fig. 1) to achieve different detection depths. The observation radii for each observation site (ranging from 40 to 300 m) were properly adjusted depending on the geological conditions (depth of the bedrock) at each site (see Table S1 in the electronic supplement). Ten receivers (seismometers) are required for such an observation system, three of which were equally spaced on the largest circle, forming an equilateral triangle. Together with the one at the center they formed one array system. Then, the three receivers located at the midpoint of each side of the large equilateral triangle and the one at the center formed another array. In a similar manner, the array with smallest radius could be constructed.

The data acquisition system consisted of a single-component velocity-type sensor with a natural period of one second, an amplifier (filter) and a digital recorder. The system was utilized to record microtremors (ambient vibrations) at each observation site, as shown in Figure 2. The specially designed amplifier (filter) extends the sensor's nature period from 1 to 5 ~ 7 s. We made simultaneous observations for 30 minutes at the eight sites for the three observation arrays. The microtremors were recorded by digital recorders with a resolution of 16 bits. The records were synchronized with the slow code generated by GPS clocks. A sampling rate of 100 Hz and a low-pass filter with a high cutoff frequency of 10 Hz were adopted.

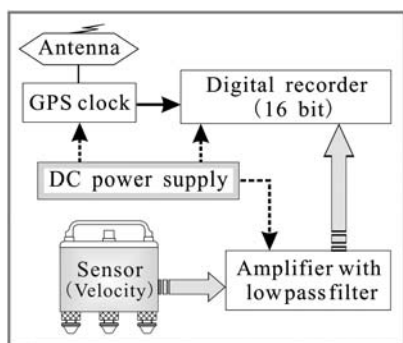
DATA ANALYSIS AND RESULTS

Data processing can be divided into two steps: (1) estimation of phase velocities of Rayleigh-wave from the vertical components of the microtremor records at the eight sites using the SPAC method (Aki, 1957; Okada *et al.*, 1987; Malagnini *et al.*, 1993), and (2) inversion to establish the *S*-wave velocity structure.

Theoretically, the spatial autocorrelation coefficient at the frequency f for the microtremors observed by the circular array is related to the phase velocity $c(f)$ via the Bessel function of the first kind and zero order (Aki, 1957; Ling, 1994; Okada, 2006):

$$\rho(f, r) = J_0[2\pi f r / c(f)]. \quad (1)$$

In this way, the phase velocity $c(f)$ of a certain frequency can be calculated by the spatial autocorrelation coefficient of



▲ **Figure 2.** Block diagram of the observation system.

the component of the wave for which the frequency is f , from the microtremors recorded with a circular array of radius r .

Specifically, we first divided the observed records of vertical components into time segments of 40.96 s for each array receiver. After removing some time segments that were clearly contaminated by instrumental or locally generated noise, we computed the amplitude spectra of the data in time windows for all three of the aperture arrays at each site. Then the power spectra densities were computed for a single 40.96 s window. Figure 3 shows the power spectra of the array microtremor records at site F16-1 ($r = 100$ and 50 m, respectively). It is shown that there is little change in the power spectra among the four stations deployed throughout the experiment, indicating that the microtremor events satisfy the properties of a stationary stochastic process.

Second, we calculated the spatial autocorrelation function for all possible station pairs of the circular array, and averaged them over many different azimuths to obtain the spatial autocorrelation coefficient. By fitting the Bessel function of the first kind and zero order, the Rayleigh-wave phase velocity dispersion curves can be obtained.

Figure 4 shows the portion of the spatial autocorrelation coefficients computed for all possible station pairs of the array at site F16-1 ($r = 200$ and 100 m). The high level of agreement among all 42 windows suggests a stationary microtremor wave field in the time domain. The average values describe a curve that resembles a zero order, first-kind Bessel function. This suggests that it is possible to substitute temporal averaging for azimuthal averaging in the computation of the correlation coefficients.

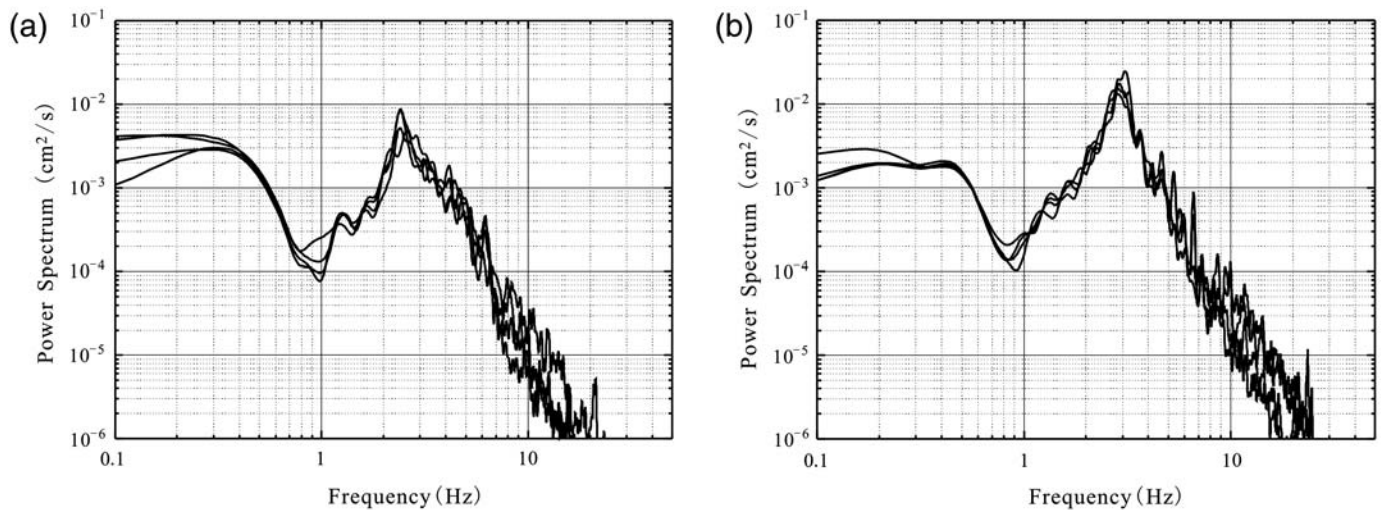
Consequently, we obtained the observed phase-velocity dispersion curves for the fundamental mode of the Rayleigh wave (Fig. 5) at all locations, with the frequency ranging between 0.3 and ~3.9 Hz.

Finally, 1D structure models down to a depth of about 3 km at these locations were established by fitting the observed and theoretical phase velocities by means of a nonlinear-inversion method known as a genetic algorithm (GA; Cho *et al.*, 1999). In one GA estimation, 5000 models were generated and their numerical simulations were performed. We selected those that gave the smallest residuals among five estimations as our final velocity model. The *P*-wave velocity and density were assumed as a function of the *S*-wave velocity by using the relationship described by Ludwig *et al.* (1970).

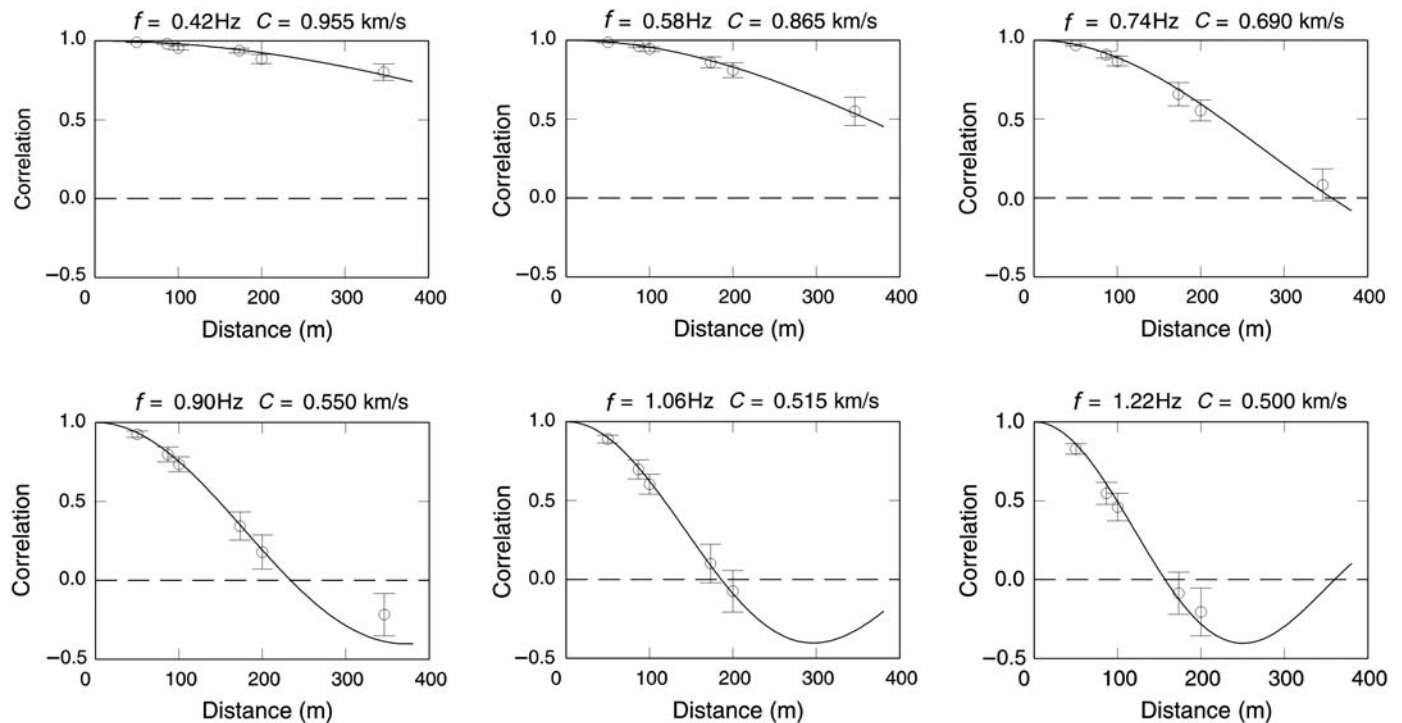
Figure 5 shows the comparisons between the observed and theoretical phase-velocity dispersion curves for the fundamental mode of the Rayleigh wave calculated from the modeled 1D structure listed in Table S2 (see supplement). The results show that the observed phase velocity dispersion curves of the Rayleigh wave can be more effectively fitted by using six or seven layers of the *S*-wave velocity model at all locations.

BEDROCK BURIAL DEPTH INTERPRETATION

Shear-wave velocity is affected not only by lithology, but also by other factors, such as the burial depth, porosity, fractures,



▲ **Figure 3.** Power spectra of the array microtremor records at site F16-1; (a) $r = 100$ m; (b) $r = 50$ m. Each curve corresponds with an observation point of the array.



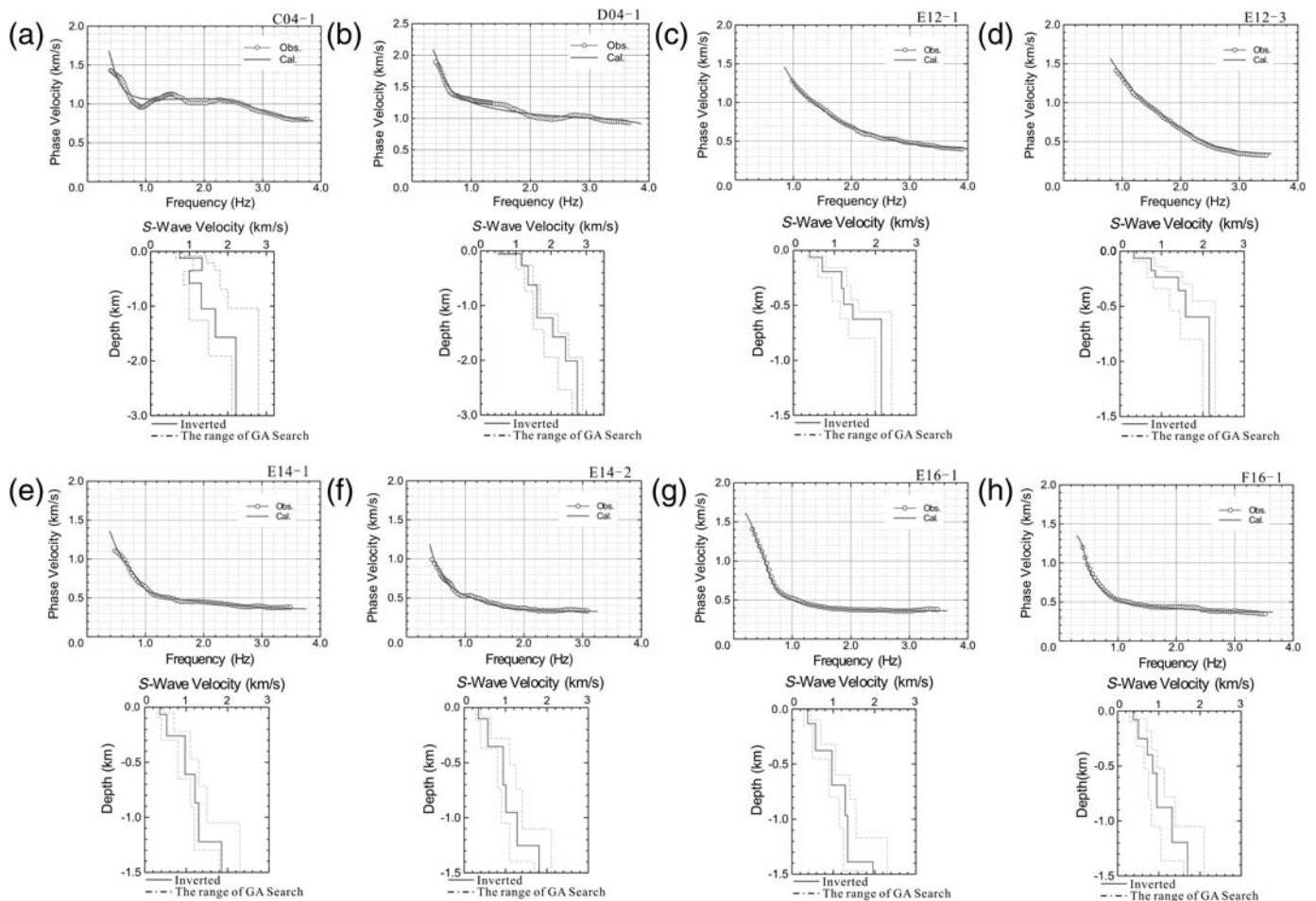
▲ **Figure 4.** An example of fitting the first kind of zero-order Bessel functions to the spatial autocorrelation coefficient at site F16-1. Solid line, the Bessel function of best fit to the coefficient; open circles with vertical bars, the average and standard deviation values at each distance.

and possibly pore pressure. It is thus difficult to determine the bedrock depth by the shear-wave velocity alone. Controlled by tectonic structures and faults, the bedrock in the area has different depth ranges in different fault blocks. Therefore, we combined the obtained shear-wave velocity profile, the well data, and the geological structure characteristics in that block to obtain the structure map of the bedrock. It is important to ensure that the interpretation result is locally consistent with

the sedimentary environment, structure, and geological characteristics of the block. Subsequently, we provided detailed descriptions of local conditions for all eight sites and our interpretation.

C04-1 and D04-1

C04-1 and D04-1 are located in the Fengtai Sag where the Cenozoic strata have the thickest rock column. The geothermal



▲ **Figure 5.** The microtremor array observation results for the eight sites; (a) C04-1, (b) D04-1, (c) E12-1, (d) E12-3, (e) E14-1, (f) E14-2, (g) E16-1, and (h) F16-1. The estimated phase velocities from the microtremor array observations (obs.) and the calculated fundamental modes (cal.) of the dispersion curves of the Rayleigh-wave are plotted across the top row. The inverted 1D *S*-wave velocity model and the ranges of genetic algorithm (GA) search are shown at the bottom.

well data indicated that more than 1000 m of the Tertiary (from Paleogene to Neogene) was deposited in the lower section of the strata. Influenced by the north-northeast-striking Huangzhuang–Gaoliying and Nanyuan–Tongxian faults, the sediment deposition center within the Fengtai Sag moved throughout geological time. The Cenozoic strata become thinner near the two major faults at both the western and eastern sides of the sag (Luo *et al.*, 2008). In short, the rocks in the area are of Quaternary, Tertiary, and Cretaceous ages. The Quaternary stratigraphic lithology is composed of interbedded layers of clay, sand, and gravel. The Neogene strata are mainly weakly cemented mudstone, siltstone, and sandy conglomerate. The Cretaceous rocks are mainly composed of mudstone, sandstone, and conglomerate (Ke, 2009a).

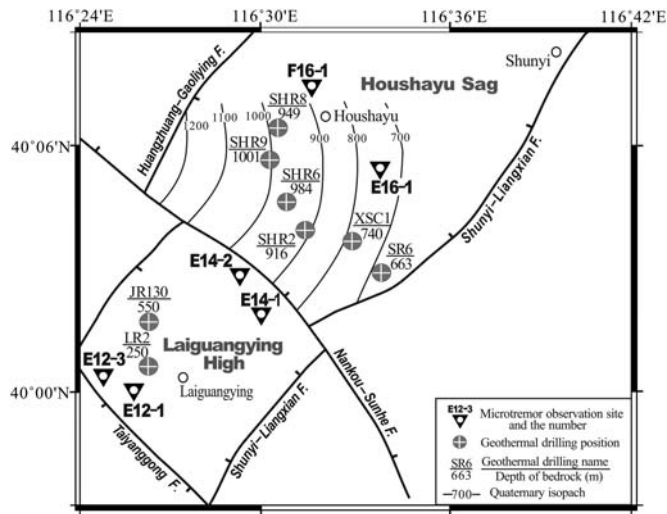
Taking into account the fact that the bedrock burial depth (1586 m) was penetrated at well JR59 (see Fig. 1), we interpreted the interface between the fifth and sixth layer at 1510 m as the top of the bedrock at the observation site C04-1 (see Table S2 in the electronic supplement and

Figure 5a). The resulting shear-wave velocity was 2.21 km/s for Cretaceous bedrock (marked with the blackbody in Table S2 in the electronic supplement), and 1.65 km/s for its overlying Upper Paleogene (E) strata, producing a velocity difference of 0.56 km/s.

D04-1 has very similar stratigraphic units (Fig. 5b) to those at C04-1. The interface between the fifth and sixth units at 1575 m was thus interpreted as the top of the bedrock, with an estimated shear-wave velocity of 2.41 km/s (see Table S2 in the electronic supplement and Figure 5b). The velocity contrast at the interface was approximately 0.36 km/s.

E12-1, E12-3, E14-1, and E14-2

Four observation sites (E12-1, E12-3, E14-1, and E14-2) were located in the fault block of the Laiguangying High. Its stratigraphic unit within the block consists of Quaternary, Jurassic, and Carboniferous–Permian rocks. Because of the lack of Tertiary rocks in the block column, the Jurassic bedrock burial depth (varying from 200 to 550 m) is much shallower than



▲ **Figure 6.** Geological structure map of the Laiguangying High and Houshayu Sag (Ke, 2009b). The isochore map for the Cenozoic strata was drafted from the geothermal drilling data.

that at the Fengtai Sag (Ke, 2009b). Existing well data (Fig. 6) shows that the bedrock top is at approximately 250 m at the LR2 well and at 550 m at JR130, suggesting shallower burial depths near the center of the Laiguangying High, and deeper burial depths toward the major faults (Huangzhuang–Gaoliying and Nankou–Sunhe).

Taking into account the well data described previously, we interpreted the interface between the second and third layers as the top of the bedrock. The corresponding bedrock burial depths are 193 m at E12-1 and 236 m at E12-3 (see Table S2 in the electronic supplement). The respective inverted shear-wave velocities of the two locations are 1.18 and 1.41 km/s.

Because of the fact that E14-1 and E14-2 were located close to the Nankou–Sunhe fault, we expected deeper burial depths for the bedrock in comparison with those at E12-1 and E12-3. Considering the bedrock burial depth range in the block, we interpreted the interface between the second and third layers as the top of the bedrock. The corresponding burial depths of the bedrock are 260 m at E14-1 and 355 m at E14-2 (see Table S2 in the electronic supplement). The inverted shear-wave velocity appears to be too low for the bedrock (0.97 km/s at E14-1 and 0.94 km/s at E14-2). However, if we take the base of the third layer as the top of the bedrock, then the inverted bedrock burial depths (610 and 703 m, respectively) are outside the depth range (200–550 m), as interpreted based on existing well data, despite the fact that the estimated shear-wave velocity (1.21 km/s at E14-1 and 1.01 km/s at E14-2) appears to be slightly more reasonable. We inspected our inversion results several times and found no issue; therefore, we interpreted the low shear-wave velocity to be caused by the heavily fractured zones related to the Nankou–Sunhe fault. It was speculated to be a fault system with a very wide fracture zone, although we did not know its exact width and location on the map. In addition, the Shunyi fault, which was not shown on the map, passes through the

two observation sites. It is highly possible that E14-1 and E14-2 are actually situated above or close to a highly fractured zone related to the fault. In the case of high lateral velocity contrast, the SPAC method generally underestimates the shear-wave velocity, leading to inaccurate depth estimation. This topic is out of the scope of the present paper.

F16-1 and E16-1

F16-1 and E16-1 are located in the Houshayu Sag (see Figs. 1 and 6, respectively), which is situated on the northern side of the Nankou–Sunhe fault. The sag was formed when the hanging wall of the fault moved downward under extension. The Nankou–Sunhe fault was very active during the Quaternary, and played a significant role in controlling the structural shape of the Houshayu Sag (Cai *et al.*, 2009). The Bouguer gravity map (Ke, 2009b) showed a low-gravity anomaly around the sag. Geothermal well data indicated very thick (approximately 1000 m) Quaternary strata in the sag (Ke, 2009b). Its lithology consists of mainly clay, sand, and sandy gravels, followed by a thick section of muddy conglomerate at its base (Cai *et al.*, 2012). Again, the entire Tertiary section is missing and the underlying bedrock column in the sag is composed of andesite, andesitic breccia, tuff sandstone, and siltstone of Upper Jurassic age (Ke, 2009b; Cai *et al.*, 2012).

Ke (2009b) made a Quaternary isochore map from the geothermal well data located mainly on the southern section of the Houshayu Sag (Fig. 6), showing a considerable change in the Quaternary thickness from east to west, but remaining almost completely constant from north to south. We used the map as a reference during our interpretation of the inversion results at F16-1 and E16-1. Considering the fact that E16-1 was located between the contours 700 and 800 m and was constrained by the well data at XSC1 (740 m) and SR6 (663 m), we interpreted the third interface at 691 m as the top of the bedrock. The resulting bedrock shear-wave velocity was 1.295 km/s. Similarly, the bedrock burial depth at F16-1 (see Table S2 in the electronic supplement) was estimated at 875 m, which was within the range of 740 m at XSC1 and 916 m at SHR2. The estimated bedrock shear-wave velocity was 1.325 km/s.

Chen *et al.* (2009) conducted the microtremor measurements from more than 600 sites, with approximately 1 ~ 2 km spacing in metropolitan Beijing, and used the horizontal-to-vertical spectral ratio (H/V) method to present the uppermost soft sediment (Quaternary) thickness map covering the entire area inside Beijing's fifth Beltway. We found that the thickness of the Quaternary strata obtained in our study at the sites of C04-1, D04-1, E12-1, and E12-3 agreed quite well with the results shown by Chen *et al.* (2009). The microtremor-derived sediment thickness better agrees with the borehole data (Ke, 2009a,b), which coincide with the major geomorphological and neotectonic expressions in metropolitan Beijing.

In summary, our inversion results show thick Cenozoic sedimentation in the Fengtai Sag. The bedrock depth is 1510 m at C04-1 and 1575 m at D04-1. In contrast, the Cenozoic sediments are only 193 m thick at E12-1 and 236 m thick

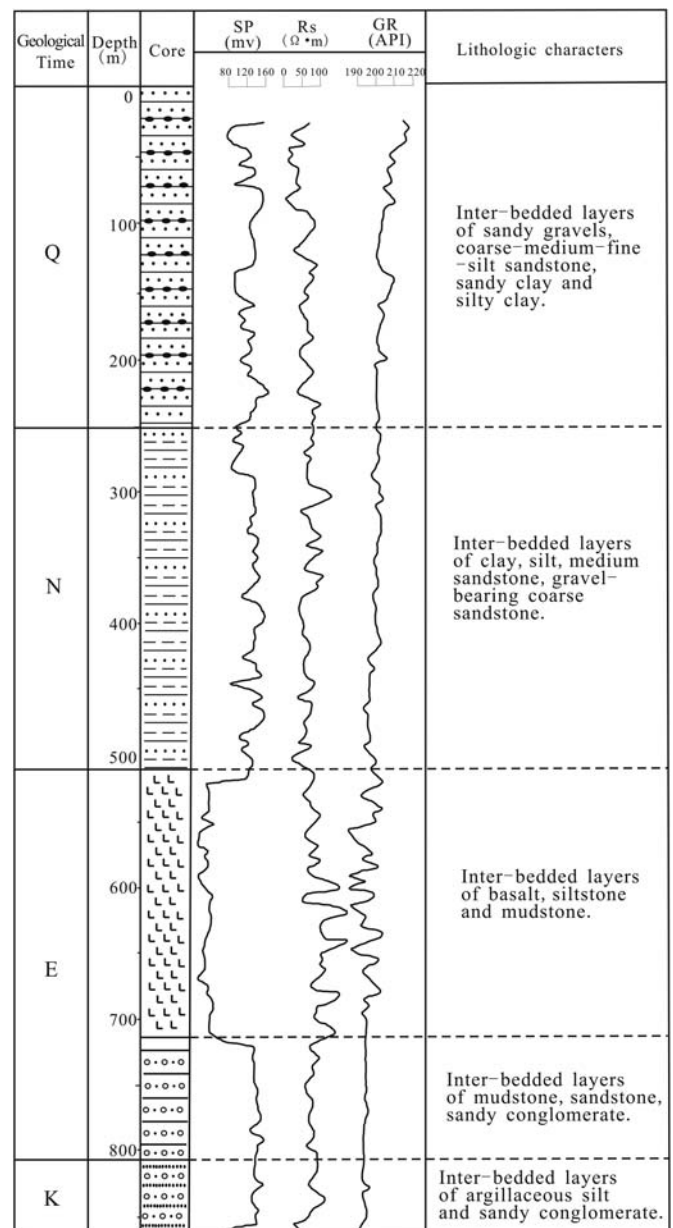
at E12-3, indicating very thin Cenozoic sedimentation in the Laiguangying High structural unit. The bedrock at the Houshayu Sag with a depth of 691 m at E16-1 and 875 m at F16-1, respectively, seems to fall somewhere in the middle. The difference between the bedrock depth at the Fengtai Sag and that at the Laiguangying High is as much as 1300 m. This was interpreted as resulting from a slip along the Taiyanggong fault (Fig. 1; Zhang and Lv, 2008). On the other hand, the Nankou–Sunhe faulting resulted in a bedrock depth difference of approximately 500 m between the Laiguangying High and Houshayu Sag to the northeast. These results of the bedrock surface depth and its difference in various tectonic units in the Beijing plain area outlined by this article are consistent with both the existing geological data and previous interpretations.

DISCUSSIONS

The shear-wave velocity for the pre-Tertiary bedrocks determined from the seismological data is generally higher than 3 km/s (Ludwig *et al.*, 1970). However, the bedrock shear-wave velocities determined at the eight observation sites within the Beijing Plain area are in the range of 1.18 to 2.41 km/s, which is much lower than expected.

Within the Beijing Plain area, almost all the Jurassic (J), Cretaceous (K), and Tertiary (E ~ N) strata are continental deposits. Similar terrestrial sources and the depositional environment during the geological period resulted in smaller lithological differences at the geological interface, making it difficult to determine them. A typical example of the rock property characteristics can be seen at the X5 well located in the Beijing Depression (Fig. 1). The drilling results (Fig. 7) show a dense layer of basalt overlying a sequence of interbedded mudstone and siltstone at the base of the Cenozoic section. There is little contrast in spontaneous potential, resistivity, and natural gamma ray logs at the Cenozoic–Cretaceous interface. All the evidence shows a relatively small shear-wave velocity contrast at the Cenozoic–Cretaceous interface. Therefore, it indicates a slow shear-wave velocity in the Cretaceous bedrock, which is largely in agreement with our microtremor inversion results.

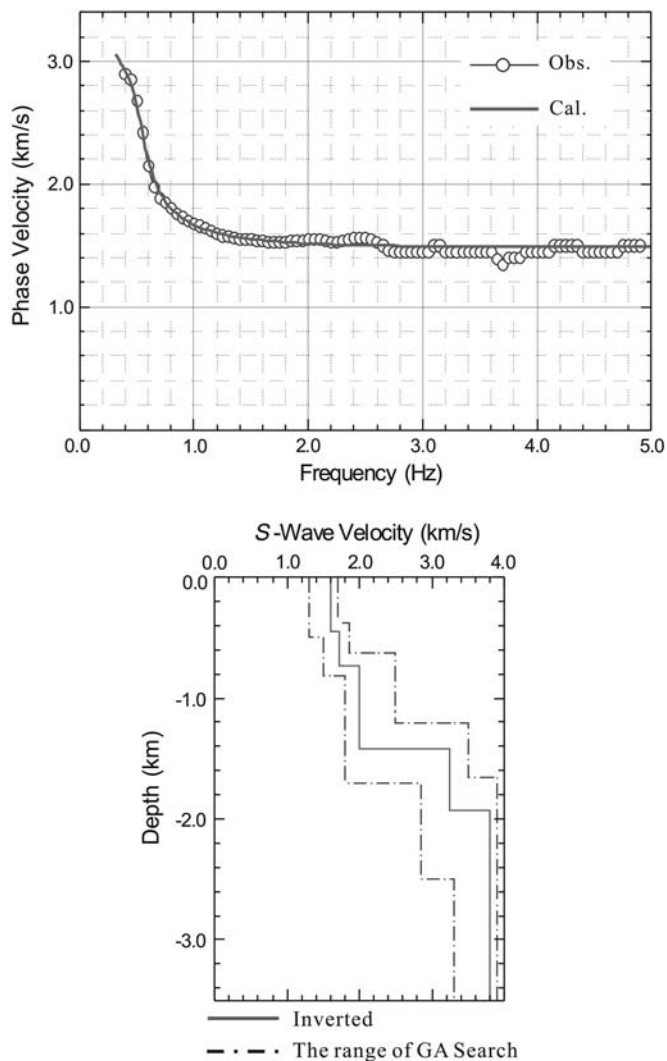
On the other hand, our inversion result at a microtremor observation point in the Beijing Fangshan area (located within the Jingxi Uplift structural unit on the west side of the Huangzhuang–Gaoliying fault) indicated a much faster shear-wave velocity (> 3.25 km/s) for the pre-Tertiary bedrock (see Fig. 8 and Table S3 in the electronic supplement). The observation point is located close to the northwest boundary of the Fangshan metamorphic core complex (FMCC). Massive Cretaceous granodiorite directly overlying the older Upper Proterozoic and Lower Paleozoic strata with a total thickness of more than 5000 m is exposed at the surface, after having being lifted during the orogenic movement and eroded since that time (Song, 1996). Our inverted shear-wave velocity is almost 1.6 km/s at the surface (see Table S3 in the electronic supplement). We also observed a significant shear-wave velocity contrast of 1.25 km/s at the interface between the



▲ **Figure 7.** Lithology column and well logs at well X5 (Fig. 1; Cai *et al.*, 2010). SP, spontaneous potential; Rs, resistivity; GR, natural gamma ray.

third and fourth layers (1420 m), and the shear-wave velocity below the interface is as high as 3.25 km/s. Such a shear-wave velocity structure may be related with a special regional structural relationship developed during formation of FMCC, which possibly implies the northern FMCC's extensional wedge with detachment zone occurring between the upper the Late Mesozoic and the lower the Late Precambrian-Paleozoic stratigraphic layers, that is, it is highly possible that this interface represents the boundary between the Late Mesozoic (K) and Proterozoic-Paleozoic strata.

As indicated by the above example, the shear-wave velocity of the bedrock within the Jingxi Uplift is much faster than that in the Beijing Plain area. In general, shear-wave velocity



▲ **Figure 8.** Microtremor observation results at Fangshan located within the Jingxi Uplift. The means of the diagrams above and below are the same as those in Figure 5.

of sedimentary rocks increases with age and burial depth. However, igneous and metamorphic rocks may not exactly follow this trend. The Qingbaikou (Qn), Jixian (Jx), and Changcheng (Ch) systems of the Upper Proterozoic age are the oldest strata in the Beijing area, with shear-wave velocities faster than 3.0 km/s. Hot water has been extracted from these rock strata for civilian use for years. In contrast, the Ordovician (O) and Cambrian (Є) rocks have a relatively slow shear-wave velocity of about 2.0 km/s. Several previous studies have shown that the Ordovician and Cambrian formations in the Beijing plain contain aquifers that can be used for daily drinking water (e.g., Ke, 2009a). This is most likely due to the fact that Beijing possesses a unique geotectonic position, strong compression, extension, and large-scale tectonic activity in the Mesozoic period. Consequently, the Ordovician and Cambrian formations suffered a strong tectonic deformation of compression and extension, producing abundant fractures in the rock mass, followed by water filling (Song, 1996). It is well known that water-filled frac-

tures will greatly reduce the shear-wave velocity. The situation in the Beijing Plain area is similar to that described above. However, due to the fact that there are two sets of north-northeast and northwest fractures in many faults, the influence of the fracture zone is more prominent, resulting in much lower strata velocity. This phenomenon is in strong agreement with our results.

When using the microtremor method, we must select one of the velocity interfaces as the top of the bedrock to determine the bedrock burial depth. In most cases, we are able to roughly determine the bedrock burial depth range in the area, based on existing geological or well data. In order to be consistent with existing data, we interpret an interface with a relatively larger velocity contrast within the depth range to be the Cenozoic bedrock (Pre-Tertiary) interface. At present, we have completed approximately 160 microtremor surveys for the bedrock burial depth estimation. Validation using other geological data, for example drilling, shows relative errors of less than 10% in our inversion results. In the cases for which there is a large shear-wave velocity contrast at the Cenozoic–Pre-Tertiary interface, for example, Cenozoic clay and sandy sediments situated on the top of Jurassic igneous rocks, the relative errors are further reduced to less than 5%.

Our results show that the shear-wave velocity for the pre-Tertiary bedrock may vary significantly from one geological structure unit to another, and may even vary with burial depth within the same geological unit. Therefore, it is difficult if not possible to identify the Cenozoic–pre-Tertiary interface based on shear-wave velocity alone. Available geological data, for example existing drilling results, tectonic events, are necessary for the reliable interpretation of the Cenozoic–pre-Tertiary interface and its correlation among the geological structure units. On the other hand, it should be noted that the microtremor survey method is strictly applicable to horizontally layered structures, and the method tends to underestimate shear-wave velocities in cases involving strong lateral velocity contrasts. As shown earlier, the inverted shear-wave velocity using this method is unreliable at observation sites E14-1 and E14-2, which are seated above a highly fractured zone associated with the Nankou–Sunhe fault.

CONCLUSIONS

This paper reports our first attempt to utilize the microtremor-array analysis technique to estimate shear-wave velocity profiles at eight observation sites in the Beijing Plain area. Integrating the existing drilling results and other geological data from the area, we successfully obtained the bedrock depth, which plays a significant role in interpreting the thickness of the Cenozoic. We also demonstrated that increased data density may lead to an improved accuracy in bedrock depth mapping. It has been shown that this method is especially useful and effective in densely populated urban areas where heavy traffic and various sources of noises exist, such as in Beijing. The information is deemed very useful for understanding the geological structures, regional tectonics, and practical geotechnical problems involved in civil geological engineering in and around Beijing City. ☒

ACKNOWLEDGMENTS

The authors are very grateful to two anonymous reviewers for their thorough reading and constructive comments and suggestions, which greatly aided us in improving the manuscript. We also thank the Editor in Chief Jonathan Lees and Zhigang Peng for their critical review of this paper. This research is financially supported by the Chinese Academy of Sciences (KZCX2-EW-107) and National Natural Science Foundation of China (Grant Number 41274143).

REFERENCES

- Aki, K. (1957). Space and time spectra of stationary stochastic waves with special reference to microtremors, *Bull. Earthq. Res. Inst.* **35**, 415–456.
- Aki, K. (1965). A note on the use of microseisms in determining the shallow structures of the earth's crust, *Geophysics* **30**, 665–666.
- Cai, X., G. Guo, Y. Luan, Z. Sun, Y. Liang, and L. Jian (2010). Forming time for the Yongdinghe River, *Quaternary Sci.* **30**, 167–174.
- Cai, X., Y. Luan, G. Guo, and H. Liu (2009). Geological system in Beijing plain area, *City Geol.* **4**, 6–12.
- Cai, X., Y. Luan, Y. Liang, and J. Zhuang (2012). Geological characteristics and origin of the mud gravel stratum in Beijing Plain area, *Geol. Surv. Res.* **33**, 309–314.
- Chen, Q., L. Liu, W. Wang, and E. Rohrbach (2009). Site effects on earthquake ground motion based on microtremor measurements for metropolitan Beijing, *Chin. Sci. Bull.* **54**, 280–287.
- Cho, I., I. Nakanishi, S. Q. Ling, and H. Okada (1999). Application of Forking Genetic Algorithm fGA to an exploration method using microtremors, *Geophys. Explor. (Butsuri-Tansa)* **52**, 227–246.
- Horike, M. (1985). Inversion of phase velocity of long-period microtremors to the S-wave-velocity structure down to the basement in urbanized areas, *J. Phys. Earth* **33**, 59–96.
- Jiao, Q., and Z. Qiu (2006). Research progress of major active faults in Beijing plain area, in *Crustal Structure and Crustal Stress*, The Institute of Crustal Dynamics, Chinese State Seismological Bureau, Earthquake Press, Beijing, Vol. 18, 72–84.
- Kawase, H., T. Satoh, T. Iwata, and K. Irikura (1998). S-wave velocity structures in the San Fernando and Santa Monica areas, in *Proc. of the 2nd International Symposium on Effects of Surface Geology on Seismic Motions*, Tokyo, Japan, Vol. 2, 733–740.
- Ke, B. (2009a). Characteristics of geothermal geology in the northwestern part of the urban Beijing geothermal field, *Geoscience* **23**, 49–56.
- Ke, B. (2009b). Geothermal and geological features of Sunhe fault in the northern part of Beijing plain, *Geoscience* **23**, 43–48.
- Ling, S. Q. (1994). Research on the estimation of phase velocities of surface waves in microtremors, *Ph.D. Thesis*, Hokkaido University, Japan.
- Ludwig, W. J., J. E. Nafe, and C. L. Drake (1970). Seismic refraction, in *The Sea*, A. Maxwell (Editor), Vol. 4, 53–58, Wiley Inter-Science, New York.
- Luo, M., S. Zhang, J. Ren, Y. Wang, and Y. Zhang (2008). Cenozoic sedimentary and tectonic evolution in Beijing down-warped basin, in *Crustal Structure and Crustal Stress*, The Institute of Crustal Dynamics, Chinese State Seismological Bureau, Vol. 20, 62–74, Earthquake Press, Beijing.
- Malagnini, L., A. Rovelli, S. E. Hough, and L. Seeber (1993). Site amplification estimates in the Garigliano valley, central Italy, based on dense array measurements of ambient noise, *Bull. Seismol. Soc. Am.* **83**, 1744–1755.

- Matsushima, T., and H. Okada (1990). Determination of deep geological structures under urban areas using long-period microtremors, *Geophys. Explor.* **43**, 21–33.
- Ohori, M., A. Nobata, and K. Wakamatsu (2002). A comparison of ESAC and FK methods of estimating phase velocity using arbitrarily shaped microtremor arrays, *Bull. Seismol. Soc. Am.* **92**, 2323–2332.
- Okada, H. (2003). *The Microtremor Survey Method*, Geophysical Monograph Series, Society of Exploration Geophysicists Monograph, 12, 135 pp.
- Okada, H. (2006). Theory of efficient array observations of microtremors with special reference to the SPAC method, *Explor. Geophys.* **37**, 73–85.
- Okada, H., T. Matsushima, and E. Hidaka (1987). Comparison of spatial auto correlation method and frequency–wavenumber spectral method of estimating the phase velocity of Rayleigh waves in long-period microtremors, *Hokkaido Daigaku Chikyu Butsurigaku Kenkyu Hokoku/Geophysical Bulletin of Hokkaido University* **49**, 53–62 (in Japanese with English abstract).
- Okada, H., T. Matsushima, T. Moriya, and T. Sasatani (1990). An exploration technique using long-period microtremors for determination of deep geological structures under urbanized areas, *Geophys. Explor. (Butsuri-Tansa)* **43**, 402–417 (in Japanese with English abstract).
- Satoh, T., H. Kawase, and S. Matsushima (2001). Estimation of S-wave velocity structures in and around the Sendai basin, Japan, using array records of microtremors, *Bull. Seismol. Soc. Am.* **91**, 206–218.
- Song, H. (1996). Characteristics of Fangshan metamorphic core complex, Beijing and a discussion about its origin, *J. China Univ. Geosci.* **10**, 149–158.
- Zhang, R., and J. Lv (2008). Research on urban geological survey inside the 6th ring road of Beijing, *City Geol.* **3**, 5–9.

Peifen Xu

Key Laboratory of Engineering Geomechanics
Institute of Geology and Geophysics
Chinese Academy of Sciences
Beijing 100029, China
pfxu@mail.iggcas.ac.cn

Suqun Ling

Geo-Analysis Institute Co. Ltd.
20-13, Nakacho 3-chome, Koganei
Tokyo 184-0012, Japan
sqling818@yahoo.co.jp

Weiyuan Ran

Qingxiao Liu
Beijing Institute of Geo-exploration Technology
China Geological Survey Bureau
Beijing 102218, China
ranweiyuan@sina.com
liuqxiao@sohu.com

Jinguang Liu

AVIC Geotechnical Engineering Institute Co. Ltd.
56 Zhichunlu, Haidian District
Beijing 100098, China
ljg0901@vip.sina.com

Electronic Supplement to

Estimating Cenozoic Thickness in the Beijing Plain Area Using Array Microtremor Data

by Peifen Xu, Suqun Ling, Weiyan Ran, Qingxiao Liu, and Jinguang Liu

Table S1. Observation Radius (m) Used for Microtremor Measurements at Different Sites

Site	Longitude (E)	Latitude (N)	Observation Radius (m)		
			r1	r2	r3
D04-1	116°14'26.8"	39°52'45.6"	75	150	300
C04-1	116°17'56.0"	39°51'31.3"	40	80	180
E12-1	116°25'52.1"	40°00'06.9"	50	100	180
E12-3	116°24'48.0"	40°00'22.7"	50	100	160
E14-1	116°29'55.5"	40°01'59.1"	50	100	200
E14-2	116°29'15.1"	40°02'58.2"	50	100	200
E16-1	116°33'48.1"	40°05'35.9"	50	100	200
F16-1	116°31'33.5"	40°07'36.8"	50	100	200

Table S2. Inverted *S*-wave Velocity Structure at the Observation Sites

Site	V_s (km/s)	V_p (km/s)	ρ (g/cm ³)	H(m)	T
D04-1	0.53	1.91	1.894	55	Q
	1.16	2.528	2.119	275	N+E
	1.35	2.789	2.179	625	
	1.6	3.143	2.247	1225	
	2.05	3.773	2.358	1575	
	2.41	4.284	2.436	2010	K
	2.745	4.783	2.511	∞	
C04-1	0.75	2.139	1.986	115	Q
	1.33	2.762	2.173	350	N+E
	1	2.384	2.073	560	
	1.315	2.736	2.168	1010	
	1.65	3.211	2.26	1510	
	2.21	4.001	2.394	∞	K
E12-1	0.4	1.798	1.834	65	Q
	0.71	2.096	1.968	193	

	1.18	2.55	2.125	347	J
	1.23	2.62	2.142	492	
	1.45	2.929	2.206	627	
	2.15	3.918	2.381	∞	
E12-3	0.34	1.732	1.804	65	Q
	0.75	2.139	1.986	176	
	0.855	2.228	2.022	236	
	1.41	2.869	2.195	356	J
	1.585	3.116	2.242	596	
	2.15	3.918	2.381	∞	
E14-1	0.367	1.754	1.814	65	Q
	0.53	1.91	1.894	260	?
	0.97	2.362	2.065	610	?
	1.21	2.59	2.135	868	
	1.3	2.722	2.165	1223	
	1.85	3.487	2.31	∞	
E14-2	0.348	1.732	1.804	103	Q

	0.57	1.944	1.909	355	?
	0.94	2.325	2.054	703	?
	1.01	2.391	2.076	953	
	1.28	2.695	2.16	1253	
	1.815	3.429	2.299	∞	
E16-1	0.382	1.776	1.824	130	Q
	0.576	1.944	1.909	376	
	0.975	2.362	2.065	691	
	1.295	2.709	2.163	968	J
	1.35	2.789	2.179	1388	
	1.96	3.645	2.337	∞	
F16-1	0.38	1.776	1.824	80	Q
	0.505	1.885	1.881	250	
	0.725	2.106	1.972	400	
	0.855	2.228	2.022	565	
	0.95	2.338	2.058	875	
	1.325	2.749	2.171	1195	J

1.7	3.278	2.272	∞		
-----	-------	-------	----------	--	--

V_s : S -wave velocity, V_p : P -wave velocity. Density ρ and the bottom depth of the layer H are the model parameters. The numbers in bold and italics, such as **1575** and **2.410**, represent the burial depth and shear-wave velocity of the bedrock respectively. T represents estimated geological time: Q: Quaternary, N: Neogene, E: Paleogene, K: Cretaceous, J: Jurassic.

Table S3. Inverted S -wave velocity structure at Fangshan located within the Jingxi Uplift

V_s (km/s)	V_p (km/s)	ρ (g/cm ³)	H(m)	T
1.6	3.143	2.247	450	K
1.71	3.292	2.275	735	
2	3.702	2.346	1420	O、 \in
3.25	5.661	2.643	1930	Qn、Jx、Ch
3.8	6.775	2.885	∞	

T denotes the estimated geological time, K: Cretaceous, O: Ordovician, \in : Cambrian, Qn, Jx and Ch: Upper Proterozoic. The meanings of the rest parameters are the same as those in Table S2.